A Liouville optimal control framework in prostate cancer

H. Edduweh † S. Roy*

Abstract

In this work we present a new stochastic framework for obtaining optimal treatment regimes in prostate cancer. We model the realistic scenario of randomized clinical trials for incorporating randomness related to interaction between a prostate cancer cell and androgen cell quota, due to cancer heterogeneities, across different patients in a given group, using a Liouville partial differential equation. We then solve two optimization problems: one for determining the model parameters to fit the measured data and the second to determine the optimal androgen deprivation therapy. The optimization problems are implemented using a positive, stable, and conservative finite volume solver for the Liouville equations and the projected non-linear conjugate gradient method. Several numerical results, including comparison with ordinary differential equations modeling framework, demonstrate the robustness and accuracy of our proposed framework to obtain optimal treatment regimes in real time.

Keywords. Liouville equation, non-linear constrained optimization, androgen deprivation therapy, finite-volume method

AMS subject classification. 65B99, 65H10, 65K10, 90C30

1 Introduction

Prostate cancer is one of the most common and dangerous type of non-skin cancer, and is considered the second leading cause of death among men in the United States [1]. One out of every six men is estimated to be diagnosed with prostate cancer at some point in their life [2]. According to the American Cancer Society, there are around 268,490 new cases of prostate cancer in the United States, with 34,500 deaths in 2022 [3]. There are more than 3.1 million American men currently living with prostate cancer, which is nearly equal to the population of Chicago, Illinois. Globally, prostate cancer is becoming more common, although it is particularly prevalent in poorer countries [4]. The World Health Organization

[†]Department of Mathematics, University of Texas at Arlington, 411 S. Nedderman Drive, Arlington, 76019, Texas, USA. email: husseinsaid.edduweh@mavs.uta.edu

^{*(}Corresponding author) Department of Mathematics, University of Texas at Arlington, 411 S. Nedderman Drive, Arlington, 76019, Texas, USA. e-mail: souvik.roy@uta.edu

reported 9.6 million cancer deaths and 18.1 million new cancer cases in 2018. By the year 2040, it is expected that there will be 29.5 million new cases of cancer and 16.5 million deaths [5]. Therefore, the disease remains a highly discussed and researched topic in cancer studies [6].

Prostate cancer begins when some of the cells in the prostate gland start growing uncontrollably. It usually starts as a tumor without any signs or symptoms in young men, typically between the ages of 20 and 30. However, the problem is that symptoms only become noticeable after a long time, when the disease has already become dangerous. This means that by the time symptoms appear, the available treatment options for the patient are reduced, and the chances of survival are also lower [7, 8]. Although it is difficult to determine the exact causes of prostate cancer, age, race, and inherited factors are the most strongly established risk factors for it [9]. Thus, it is imperative to determine fast and effective treatment strategies for prostate cancer patients.

Doctors and researchers began to study the growth and effects of prostate cancer, and most studies and research were done in clinics. However, there are many challenges exist in clinical prostate cancer research. Some of them require clinical studies to understand the complex mechanisms of cancer and associated treatments. Another significant clinical challenge is obtaining an effective treatment strategy for each patient individually, or at least identifying a subset of patients who could benefit from a particular treatment. In addition, testing even one therapy during clinical trials is costly. These obstacles show the necessity of continuous research efforts to improve our understanding of prostate cancer and optimize treatment options for better patient results. There is a significant lack of detailed knowledge of the intricate mechanisms behind prostate cancer and the results of different therapies, and it is for this reason that some researchers have found new research methods using mathematical models to more effectively understand how prostate cancer progresses [10].

In the past years, a lot of mathematical models have been created and analyzed through collaborations with doctors to explore various aspects of prostate cancer, such as treatment choices and timetables for those treatments [11]. Through these collaborations, important discoveries have been made about how prostate cancer develops and changes over time. In the most notable of these discoveries, the authors in [11] created a simple model to describe and explain how prostate cancer grows and progresses. In [12], the authors formulated mathematical models to determine prostate cancer growth while on intermittent androgen therapy. The authors in [13] developed a mathematical model of the cancer with the treatment of androgen deprivation therapy, and this is the first clinically validated dynamical model for the disease. In [14], the authors built a new population model for vaccination and androgen deprivation therapy. The authors in [15] introduced a two-sub-population model for prostate cancer undergoing androgen suppression therapy. For other models, see e.g., [16, 17, 18].

The success of some previous works [15, 10] led to the development of several models to study the cancer's progression and devise treatment strategies. One of the frequently used methods for prostate cancer treatment is androgen deprivation therapy (ADT), which uses drugs to block or lower levels of androgen and starve the prostate cancer cells of androgen. This method was based on the significant cancer research discovery made by the authors in [19]. They found that removing the testicles (castration) can help reduce the size of prostate tumors. This discovery highlighted the significant role of androgen, a male sex hormone, in

the growth of prostate cancer cells. Their research opened the possibility of treating some cancers using chemical treatments, making this an essential development in the field.

Typically, ADT thrives at the beginning of treatment because it targets the primary tumor cells that rely on androgen for their growth. However, in many cases, ADT has some side effects [20], like relapse of the cancer. This happens because, after a few years, the androgen-dependent (AD) tumor cells resist treatment and transform into androgenindependent (AI) cells. These AI cells can continue multiplying even in an environment with limited androgen availability [21]. Some research indicates that only specific groups of patients may experience benefits from intermittent androgen deprivation therapy, but the determination of those specific groups is still an ongoing process [22, 23]. Although mathematical models have suggested that intermittent androgen deprivation therapy might extend the time until androgen-independent relapse, there is currently no solid proof from clinical trials to support this claim [24]. Moreover, doctors have no agreement about the treatment's duration or intervals [25]. The results shown in these studies show that prostate cancer can go into near extinction during the on-treatment interval before coming back during the off-treatment break. Also, the mechanism used for the method to incorporate androgen into growth and death rates is ineffective when androgen independence (AI) cells overtake androgen dependence (AD) cells. Thus, developing and assessing the optimal ADT method for prostate cancer is essential.

Most of the previous optimal control models, for cancer therapy in different cancer types, had the objective to minimize total tumor volume. The authors in [26] provided the first cancer treatment applications of optimal control theory. The optimal dose schedule is considered good when the goal of the therapy is to reduce the variance in tumor burden over a period of time. Over time, researchers have applied optimal control theory to explore various cancer treatments, including chemotherapies, inhibitors, immunotherapy, and radiotherapy (see e.g.,[27, 28, 29]). In context of prostate cancer, there has been a growing interest in using optimal control to find the best schedule of androgen-dependent therapy [30, 31]. The authors in [32] used optimal control theory to find the best treatment schedule, using abiraterone, for metastatic castrate resistant prostate cancer patients. There are also some clinical trials that support optimal ADT for prostate cancer [33, 34]. This work presents a new optimal control framework for determining the best ADT for a prostate cancer patient.

An important goal of mathematical models in prostate cancer is to be able to provide accurate patient classifications for evaluating treatment efficacies in clinical trials [11]. A common protocol for assessing clinical trial outcomes with various treatments is the use of randomized trials [35, 36, 37]. In this setup, participants are randomly grouped together into various subgroups and prescribed different treatments to assess the behavior and outcomes. The treatments are administered based on certain features, classifying the different subgroups and, for this purpose, it is important to identify the dynamical behavior of the prostate cancer mechanism. Since, individuals in a particular subgroup exhibit different cancer characteristics, due to the inherent heterogeneities of prostate cancer, the dynamics of prostate cancer in each of these subgroups exhibit a degree of randomness. Thus, the collective dynamics of each subgroup cannot be accurately represented using deterministic models. Since these cancer heterogeneities are one of the probable causes of clinical trial failures [38], it is important to develop an accurate and robust modeling setup for classification and evaluation of participants. One such accurate modeling framework can be obtained

through the use of random dynamical variables, governing the prostate cancer dynamics, whose evolution is given by the Liouville equations. Such equations are used in different fields like biology, finance, mechanics, and physics to describe how density functions change over time. These equations help us understand the collective behavior of individuals in non-interacting systems [39].

Effects and response to treatments can be modeled as optimal control problems governed by Liouville equations, where the control represents the drug dosage/frequency and its success in treating prostate cancer is to measure its efficacy in driving the Liouville cancer state to a disease-free controlled state. While the focus on control problems governed by Liouville equations has been limited, there are advantages in using the Liouville framework [40, 41] for modeling and control of prostate cancer since it incorporates the behavior across multiple dynamical trajectories. This perspective is helpful for modeling systems with uncertain initial data and exploring robust control strategies and feedback mechanisms, potentially leading to new successful outcomes [42]. In this work, we develop a Liouville dynamical model to represent the prostate cancer dynamics and, furthermore, formulate and implement an optimal control strategy for ADT in prostate cancer.

The paper is organized as follows: In the next section, we develop a Liouville model for prostate cancer dynamics. Section 3 presents the parameter estimation and optimal control problems with the Liouville equations. Section 4 presents some theoretical results about the optimization problems. In Section 5, we present some numerical schemes to solve the Liouville optimality systems. Section 6 is devoted to the numerical results with our proposed Liouville framework. A section of conclusions and acknowledgement concludes the work.

2 A Liouville model for prostate cancer

We start off with an ODE-based mathematical cell quota model (Figure 1), proposed by [13], to describe the dynamics of prostate cancer, where the model variables are as follows

 $X_1(t)$: Androgen dependent (AD) - cells

 $X_2(t)$: Androgen independent (AI) - cells

Q(t): The cell quota for androgen - nM

t: Time - /day

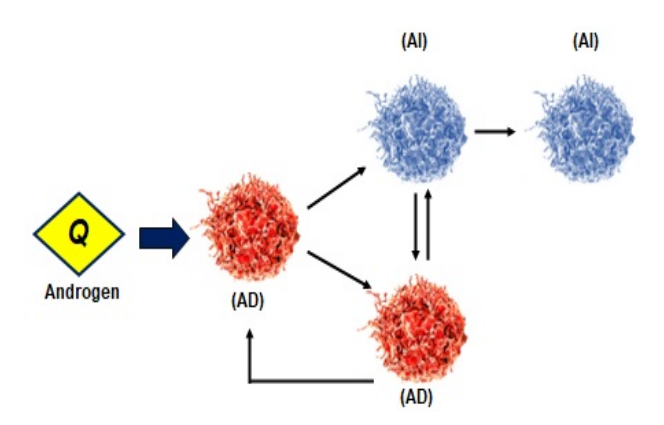


Figure 1: Schematic of the processes that occur in the model

The AD and AI cell populations are modeled by

$$\frac{dX_1}{dt} = \mu_m \left(1 - \frac{q_1}{Q} \right) X_1 - d_1 X_1 - m_1(Q) X_1 + m_2(Q) X_2,
\frac{dX_2}{dt} = \mu_m \left(1 - \frac{q_2}{Q} \right) X_2 - d_2 X_2 - m_2(Q) X_2 + m_1(Q) X_1.$$
(1)

The proliferation rate of the AD cell population is zero when Q(t) is at the minimum cell quota q. As Q(t) increases, the growth rate approaches its maximum value μ_m . The AD cell population's apoptosis rate and the AI population's net growth rate, excluding mutation, are constant. We also have the following expressions for the AD to AI mutation rate, $m_1(Q)$, and the AI to AD mutation rate $m_2(Q)$

$$m_1(Q) = c_1 \frac{k_1^n}{Q^n + k_1^n},$$

$$m_2(Q) = c_2 \frac{Q^n}{Q^n + k_2^n}.$$
(2)

We remark that $m_1(Q)$ is low for normal androgen levels and high for low androgen levels. In contrast, $m_2(Q)$ is high for normal androgen levels and low for low androgen levels, where n is the Hill's coefficient that describes the cell switching sensitivity to the cell quota level. We considered n = 1 for ultra sensitivity [43]. The cell quota for androgen within the AD cells is modeled by

$$\frac{dQ}{dt} = v_m \frac{q_m - Q}{q_m - s} \frac{A}{A + v_h} - \mu_m(Q - s) - bQ \tag{3}$$

2.1 The non-dimensional modeling

This section will convert the system from its current form with specific values to a non-dimensional form. That has two purposes: First, it helps simplify our equations by grouping parameters, making them cleaner and easier to handle. Second, non-dimensionalization is often done to reduce the computational cost of solving the system and guarantee the numerical algorithms' stability. We non-dimensionalize the ODE system using the following

non-dimensionalized states, time variables, and parameters:

$$X_{1}^{*} = l_{1}X_{1} \rightarrow X_{1} = \frac{X_{1}^{*}}{l_{1}}, \quad X_{2}^{*} = l_{2}X_{2} \rightarrow X_{2} = \frac{X_{2}^{*}}{l_{2}}$$

$$Q^{*} = l_{3}Q \rightarrow Q = \frac{Q^{*}}{l_{3}}, \qquad t^{*} = l_{4}t \rightarrow t = \frac{t^{*}}{l_{4}}$$

$$(4)$$

The non-dimensionalized parameters will be:

$$\mu_{m}^{*} = \frac{\mu_{m}}{l_{4}}, \ d_{1}^{*} = \frac{d_{1}}{l_{4}}, \ d_{2}^{*} = \frac{d_{2}}{l_{4}}, \ q_{1}^{*} = l_{3}q_{1}, \ q_{2}^{*} = l_{3}q_{2}, \ k_{1}^{*} = l_{3}k_{1}, \ k_{2}^{*} = l_{3}k_{2},$$

$$c_{1}^{*} = \frac{c_{1}}{l_{4}}, \ c_{2}^{*} = \frac{c_{2}}{l_{4}}, \ v_{m}^{*} = \frac{l_{3}}{l_{4}}v_{m}, \ q_{m}^{*} = l_{3}q_{m}, \ s^{*} = l_{3}s, \ v_{h}^{*} = l_{3}v_{h}, \ b^{*} = \frac{b}{l_{4}}, \ A^{*} = l_{3}A.$$

$$(5)$$

Then (1)-(3) can be transformed in the following way:

$$\frac{d\frac{X_1^*}{l_1}}{d\frac{t^*}{l_4}} = \mu_m \left(1 - \frac{q_1}{\frac{Q^*}{l_3}} \right) \frac{X_1^*}{l_1} - d_1 \frac{X_1^*}{l_1} - c_1 \frac{k_1^n}{\left(\frac{Q^*}{l_3}\right)^n + k_1^n} \frac{X_1^*}{l_1} + c_2 \frac{\left(\frac{Q^*}{l_3}\right)^n}{\left(\frac{Q^*}{l_3}\right)^n + k_2^n} \frac{X_2^*}{l_2},$$

Which gives us

$$\frac{dX_1^*}{dt^*} = \frac{\mu_m}{l_4} \left(1 - \frac{l_3 q_1}{Q^*} \right) X_1^* - \frac{d_1}{l_4} X_1^* - \frac{c_1}{l_4} \frac{(l_3 k_1)^n}{Q^{*n} + (l_3 k_1)^n} X_1^* + \frac{l_1}{l_4 l_2} c_2 \frac{Q^{*n}}{Q^{*n} + (l_3 k_2)^n} X_2^*$$

Using the non-dimensional parameters, we have

$$\frac{dX_1^*}{dt^*} = \mu_m^* \left(1 - \frac{q_1^*}{Q^*}\right) X_1^* - d_1^* X_1^* - c_1^* \frac{k_1^{*n}}{Q^{*n} + k_1^{*n}} X_1^* + c_2^* \frac{Q^{*n}}{Q^{*n} + k_2^{*n}} X_2^*.$$

Using similar computations, we have

$$\frac{dX_2^*}{dt^*} = \mu_m^* \left(1 - \frac{q_2^*}{Q^*} \right) X_1^* - d_2^* X_2^* - c_2^* \frac{Q^{*n}}{Q^{*n} + k_2^{*n}} X_2^* + c_1^* \frac{k_1^{*n}}{Q^{*n} + k_1^{*n}} X_1^*,$$

$$\frac{dQ^*}{dt^*} = v_m^* \frac{q_m^* - Q^*}{q_m^* - s^*} \frac{A^*}{A^* + v_h^*} - \mu_m^* \left(Q^* - s^* \right) - b^* Q^*.$$

Without loss of generality, we can remove the * and rewrite the non-dimensional ODEs as follows

$$\frac{dX_1}{dt} = \left(\mu_m \left(1 - \frac{q_1}{Q}\right) X_1 - d_1 X_1 - m_1(Q) X_1 + m_2(Q) X_2\right) = F_1(X_1, X_2, Q, \theta), \quad X_1(0) = 1$$

$$\frac{dX_2}{dt} = \left(\mu_m \left(1 - \frac{q_2}{Q}\right) X_2 - d_2 X_2 - m_2(Q) X_2 + m_1(Q) X_1\right) = F_2(X_1, X_2, Q, \theta), \quad X_2(0) = 1$$

$$\frac{dQ}{dt} = v_m \frac{q_m - Q}{q_m - s} \frac{A}{A + v_h} - \mu_m(Q - s) - bQ = F_3(X_1, X_2, Q, \theta), \quad Q(0) = 1$$
(6)

We now consider a reduced model, corresponding to (6), wherein the AD and AI prostate cancer cells are combined together as a single cell type X. The dynamics of prostate cancer is then described through the following set of equations

$$\frac{dX}{dt} = \mu_m \left(1 - \frac{s}{Q} \right) X - dX - c \frac{k^n}{Q^n + k^n} X$$

$$\frac{dQ}{dt} = v_m \frac{q_m - Q}{q_m - s} \frac{A}{A + v_h} - \mu_m (Q - s) - bQ.$$
(7)

Such a choice is motivated by the work of the authors in [15], where they found that the reduced order model (7) matched the clinical data better than (6). In randomized clinical trials, different groups of individuals are administered different treatments to test for the outcomes in each group. Even though the individuals in a group are provided with the same treatment protocol based on similar characteristics in that group, each individual still has different cancer characteristics, which can be considered as randomness, that needs to be taken into account for obtaining accurate clinical outcomes. To model this behavior accurately, the aforementioned deterministic setup is inappropriate. Rather, one needs to consider X(0), Q(0) to be random (corresponding to different individuals in a particular group) and drawn from some appropriate distribution. This renders X, Q to be random variables. Correspondingly, the ODE system (7) represents each trajectory in the ensemble dynamics of prostate cancer, initiating from different initial conditions.

Let p(x, q, t) be the joint probability density function associated to X, Q, i.e., $\mathbb{P}(X(t) = x, Q(t) = q) = p(x, q, t)$. Then the ensemble dynamics of (7) can be represented by the following Liouville equation

$$\frac{dp}{dt} + \nabla \cdot (b(x,q)p(x,q,t)) = 0,
p(x,q,0) = p_0(x,q)$$
(8)

where

$$b(x,q) = (b_1(x,q), b_2(x,q))$$

with the initial condition at t = 0 given by $p(x, q, 0) = p_0(x, q)$, $(x, q) \in \mathbb{R}^+ \cup \{0\} \times \mathbb{R}^+ \cup \{0\}$, $\nabla \equiv (\frac{\partial}{\partial x}, \frac{\partial}{\partial q})$, and

$$b_1(x,q) = \mu_m \left(1 - \frac{s}{q} \right) x - dx - c \frac{k^n}{q^n + k^n} x$$

$$b_2(x,q) = v_m \frac{q_m - q}{q_m - s} \frac{A}{A + v_h} - \mu_m(q - s) - bq,$$
(9)

Note that b_1, b_2 are essentially the right hand sides of the ODE (7), replacing X with x and Q with q. We also remark that \mathbb{P} can be chosen as any probability density function and an accurate choice can be made by statistically analyzing the characteristics of the initial conditions of the individuals in a particular group. As a special case, if \mathbb{P} is chosen to be a Dirac delta function, then (6) reduces to (7).

3 Liouville optimization problems

3.1 Parameter estimation

Let $\theta = \{\mu_m, s, d, A\}$ be the vector of the unknown patient specific parameters in (7). The reason for this choice is because these parameters show wide variability amongst different patients. The other parameters in (7) are more specific to the cancer type and, thus, can be considered fixed and known across patients (see e.g., [17]).

Parameter	Meaning	Value and units	Reference
μ_m	Maximum proliferation rate	0.025- 0.045 /day	[44]
s	Minimum AD cell quota	0.175-0.45 nM	[45]
k	AD to AI mutation half-saturation level	0.08 nM	[13]
d	AD cell apoptosis rate	0.015- 0.02 /day	[44]
c	Maximum AD to AI mutation rate	$0.00015/\mathrm{day}$	[12]
b	Cell quota degradation rate	$0.09/\mathrm{day}$	[12]
q_m	Maximum cell quota	5 nM	[13]
v_m	Maximum cell quota uptake rate	$0.275~\mathrm{nM/day}$	[13]
v_h	Uptake rate half-saturation level	4 nM	[13]
A	Maximum serum androgen level	27-35 nM	[46]

Table 1: Biological reference range for the parameters

Our goal is to estimate θ , given some data about x, q. For this purpose, we solve the following constrained optimization problem for finding θ

$$\min_{\theta} J(p,\theta) = \frac{\alpha}{2} \int_0^T \int_{\Omega} \left(p(x,q,t) - p^d(x,q,t) \right)^2 dx dq dt + \frac{\beta}{2} \|\theta\|^2$$
 (10)

subject to the Liouville equations (8) where $\Omega = \mathbb{R}^+ \cup \{0\} \times \mathbb{R}^+ \cup \{0\}$, $p(x_1, x_2, q, 0) = p_0(x_1, x_2, q)$ in Ω , $p^d(x, q, t)$ is the probability density function of given data observations from the patient, and $\|\cdot\|$ is the standard Euclidean l^2 norm of vectors. The set T_{ad} is the admissible set of θ defined as

$$T_{ad} = \{ \theta \in \mathbb{R}^4 : \theta(i) \in [0, M_i], M_i > 0 \},$$

with M_i chosen based on the non-dimensionalized version of the observed biological reference range of the parameters, as given in Table 1.

3.2 Optimal treatment

We next consider the second optimization problem to control the Liouville prostate cancer dynamics. For this purpose, we consider a controlled Liouville equation

$$\frac{dp}{dt} + \nabla \cdot (b(x, q, u)p(x, q, t)) = 0,$$

$$p(x, q, 0) = p_0(x, q)$$
(11)

where

$$b(x, q, u) = (b_1(x, q), b_2(x, q, u))$$

with the initial condition at t = 0 given by $p(x, q, 0) = p_0(x, q)$, $(x, q) \in \mathbb{R}^+ \cup \{0\} \times \mathbb{R}^+ \cup \{0\}$, $\nabla \equiv (\frac{\partial}{\partial x}, \frac{\partial}{\partial q})$, and

$$b_{1}(x,q) = \mu_{m} \left(1 - \frac{s}{q} \right) x - dx - c \frac{k^{n}}{q^{n} + k^{n}} x$$

$$b_{2}(x,q) = v_{m} \frac{q_{m} - q}{q_{m} - s} \frac{A}{A + v_{h}} - \mu_{m}(q - s) - bq - \gamma uq.$$
(12)

Here, u(t) is a function that represents an androgen receptor blocker drug to control the androgen level Q and γ is the androgen clearance rate. Our goal is to determine the optimal dosage of u(t) that can control the androgen production in cancer cells. We look for u in the admissible set

$$U_{ad} = \{u(t) \in L^2([0,T]) : 0 \le u(t) \le u_r\}, \ \forall t \in [0,T],$$

where u_r is the maximum tolerable dose. This can be formulated through the following optimal control problem

$$\min_{u} J_{u}(p, u) = \frac{\alpha}{2} \int_{0}^{T} \int_{\Omega} \left(p(x, q, t) - p^{d}(x, q, t) \right)^{2} dx dq dt + \frac{\beta}{2} \int_{0}^{T} (u(t))^{2} dt$$
 (13)

subject to the controlled Liouville equations (11), where $p^d(x, q, t)$ is the desired distribution of the dynamics that represents a successful treatment regime.

4 Theory of the optimization problems

In this section, we present some theoretical results related to the two optimization problems (10) and (13). We start with the existence and uniqueness of the solutions of (8) and (11), whose proof can be found in [47].

Proposition 1. Let $p_0 \in H^1(\Omega)$ with $p_0 \geq 0$, $\theta \in T_{ad}$, and $u \in U_{ad}$. Then, there exists an unique non-negative solution of (8) and (11) given by $C([0,T];H^1(\Omega))$.

We also have the following conservativeness property of the Liouville equations (8) and (11).

Proposition 2. The Liouville equations (8) and (11) are conservative.

Proof. Multiplying (8) and (11) by $\psi \in H^1(\Omega)$ and integrating by parts, we obtain the following

$$\int_{\Omega} \frac{\partial p}{\partial t} \psi dx = \int_{\Omega} (bp) \cdot \nabla \psi \, dx. \tag{14}$$

Choosing $\psi = 1$, we obtain $\int_{\Omega} p(x, q, t) dx = \int_{\Omega} p_0(x) dx$ for all $t \in (0, T]$ and this proves the result.

We also have the following stability estimate of the Liouville equations (8) and (11) from [47].

Proposition 3. The solutions p_1, p_2 of (8) and (11), respectively, satisfies the following stability estimate

$$||p_i(t)||_{H^1(\Omega)} \le C_i(\theta) ||p_0||_{H^1(\Omega)} \exp\left(\int_0^T ||\nabla b||_{L^{\infty}(\Omega)} dt\right), \ i = 1, 2.$$
 (15)

where C_i is independent of p, p_0, T .

The aforementioned results implies that p as functions of θ and u is continuous. Furthermore, it can also be shown that these functions are Fréchet differentiable. We now state some properties of the functionals J, J_u , given in (10) and (13), respectively, that can be proved using the fact that the PDF p is non-negative.

Proposition 4. The objective functionals J, J_u , given in (10) and (13), are sequentially weakly lower semi-continuous (w.l.s.c.), bounded from below, coercive on T_{ad}, U_{ad} . respectively, and are Fréchet differentiable.

We finally state and prove the existence of the optimal parameter set θ^* and the optimal drug dosage concentration vector u^* in the following theorem.

Theorem 4.1. Let $p_0 \in H^1(\Omega)$ and let J, J_u be given as in (10) and (13). Then, there exists pairs $(p_1^*, \theta^*) \in C([0, T]; H^1(\Omega)) \times T_{ad}$ and $(p_2^*, u^*) \in C([0, T]; H^1(\Omega)) \times U_{ad}$ such that p_1^*, p_2^* are solutions of (8) and (11), respectively, and θ^*, u^* minimize J, J_u in T_{ad}, U_{ad} , respectively.

Proof. First, we prove the existence of minimizer of J, given in (10). Due to the fact that J_1 is bounded below, there exists a minimizing sequence $(\theta^m) \in T_{ad}$. Furthermore, J being coercive in T_{ad} , this sequence is bounded, and, thus, it contains a convergent subsequence (θ^{m_l}) in T_{ad} with $\theta^{m_l} \to \theta^*$. Correspondingly, the sequence $(p^{m_l}) = p(\theta^{m_l})$ is bounded in $L^2(0,T;H^1(\Omega))$ by (15), while the sequence of the time derivatives, $(\partial_t p^{m_l})$, is bounded in $L^2(0,T;H^{-1}(\Omega))$. Therefore, both the sequences converge weakly to p_1^* and $\partial_t p_1^*$, respectively. We, thus, obtain weak convergence of the sequence $(b(\theta^{m_k}))$ in $L^2(0,T,L^2(\Omega))$. This implies that the pair (p_1^*,θ^*) minimizes J.

The existence of a minimizer of J_u , given in (13), can be proved following the same arguments as above noting the fact that since U_{ad} is a closed subspace of a Hilbert space and J_u being coercive in U_{ad} , there exists a weakly convergent subsequence (u_{m_l}) of a minimizing sequence (u_m) for J_u , and the compactness result of Aubin-Lions [48] yields strong convergence of subsequence $(p^{m_l} = p(u_{m_l}))$ in $L^2(0, T; L^2(\Omega))$. We, thus, obtain weak convergence of the sequence $(b(u^{m_l}))$ in $L^2(0, T; L^2(\Omega))$. This implies that the pair (p_2^*, u^*) minimizes J_u .

The differentiability of J, J_u , given in (10) and (13), respectively, gives the following optimality systems:

1. Optimality system for parameter estimation:

$$\frac{dp}{dt} - \nabla \cdot (b(x, q)p(x, q, t)) = 0,$$

$$p(x, q, 0) = p_0(x, q).$$
(FOR:LIOUV)

$$\frac{dw}{dt} + b(x,q) \cdot \nabla w(x,q,t) = \alpha \left(p - p^d \right),$$

$$w(x,q,T) = 0.$$
(ADJ:LIOUV)

$$(\beta \mu_{m} - \int_{0}^{T} \int_{\Omega} \left\{ \left[\left(1 - \frac{s}{q} \right) x \cdot \frac{\partial \omega}{\partial x}, -(q - s) \cdot \frac{\partial \omega}{\partial q} \right] p(x, q, t) \right\} dx dq dt) \cdot [v_{1} - \mu_{m}] \ge 0,$$

$$(\beta s - \int_{0}^{T} \int_{\Omega} \left(\frac{\mu_{m} x}{q} p(x, q, t) \cdot \frac{\partial \omega}{\partial x} \right) dx dq dt) \cdot [v_{2} - s] \ge 0,$$

$$(\beta d + \int_{0}^{T} \int_{\Omega} \left(x p(x, q, t) \cdot \frac{\partial \omega}{\partial x} \right) dx dq dt) \cdot [v_{3} - d] \ge 0,$$

$$(\beta A - \int_{0}^{T} \int_{\Omega} \left(v_{m} \frac{q_{m} - q}{q_{m} - s} \frac{v_{n}}{(A + v_{n})^{2}} p(x, q, t) \cdot \frac{\partial \omega}{\partial q} \right) dx dq dt) \cdot [v_{4} - A] \ge 0,$$

$$(OPT:LIOUV)$$

for all $v = (v_1, v_2, v_3, v_4) \in T_{ad}$.

2. Optimality system for optimal treatment:

$$\frac{dp}{dt} - \nabla \cdot (b(x, q, u)p(x, q, t)) = 0,$$

$$p(x, q, 0) = p_0(x, q).$$
(FORU:LIOUV)

$$\frac{dw}{dt} + b(x, q, u) \cdot \nabla w(x, q, t) = \alpha \left(p - p^d \right),$$

$$w(x, q, T) = 0.$$
(ADJU:LIOUV)

$$\int_{0}^{T} \left(\beta u(t) - \int_{\Omega} \left(-\gamma q p(x, q, t) \frac{dw}{dq} \right) dx dq \right) \left[v(t) - u(t) \right] dt \ge 0, \ \forall v \in U_{ad}.$$
(OPTU:LIOUV)

5 Numerical schemes for solving the optimality systems

In this section, we present and analyze some numerical schemes to solve the two optimality systems (FOR:LIOUV)-(OPTU:LIOUV). We first note that even though the Liouville

equations (8) and (11) are theoretically setup in an unobunded domain, for practical implementation, we need to consider a large but bounded domain $\Omega = (-B, B) \times (-B, B) \subset \mathbb{R}^2$. For the initial PDF p_0 , we choose a smooth density that is numerically compactly supported in Ω . We then solve (8) and (11) in $\Omega \times [0, T]$, choosing homogeneous Dirichlet boundary conditions on $\partial\Omega$. Using the results and techniques proposed in [47, 49], one can prove existence and uniqueness of smooth solutions of (8) and (11) in $\Omega \times [0, T]$. We also choose the final time T such that the solutions of the Liouville equations (8) and (11) are still contained in Ω away from its boundary.

We now consider a numerical grid that partitions Ω in $N_x \times N_x$, with $N_x > 1$, equally-spaced non-overlapping square cells of side length $h = 2B/N_x$. On this grid, we develop a cell-centered finite-volume scheme with the PDF p and its adjoint w defined at the centers of the square cells. These nodal points are given by

$$x^i := \left(i - \frac{1}{2}\right) h - B,$$
 $q^j := \left(j - \frac{1}{2}\right) h - B.$

Therefore, the elementary cell is defined as

$$\omega_h^{ij} := \left\{ (x,q) \in \Omega \quad \middle| \quad x \in \left[x^i - \frac{h}{2}, x^i + \frac{h}{2} \right], \quad q \in \left[q^j - \frac{h}{2}, q^j + \frac{h}{2} \right] \right\}.$$

This results in the computational domain as given below

$$\Omega_h = \bigcup_{i,j=1}^{N_x} \omega_h^{ij}.$$

In a similar way, the time interval [0, T] is divided in $N_t > 1$ subintervals of length $\Delta t = \frac{T}{N_t}$ and the points t^k are given by

$$t^k := k\Delta t, \qquad k = 0, \dots, N_t.$$

Then the time grid is given by $\Gamma_{\Delta t} := \{t^k \in [0, T], k = 0, \dots, N_t\}$. Thus, corresponding to the space-time cylinder $Q := \Omega \times [0, T]$ we have the numerical grid as $Q_{h, \Delta t} := \Omega_h \times \Gamma_{\Delta t}$.

We now define the cell average of the PDF p (and any other integrable function) on the cell with centre (x^i, q^j) at time t^k as follows

$$\bar{p}_{i,j}^k = \frac{1}{h^2} \int_{x^{i-1/2}}^{x^{i+1/2}} \int_{q^{j-1/2}}^{q^{j+1/2}} p(x,q,t^k) \, dq \, dx. \tag{16}$$

The initial condition is then given by

$$\bar{p}_{i,j}^0 = p_{i,j}^0 = \frac{1}{h^2} \int_{x^{i-1/2}}^{x^{i+1/2}} \int_{q^{j-1/2}}^{q^{j+1/2}} p_0(x,q) \, dq \, dx.$$

In the aforementioned finite-volume setting, the unknown variables are the cell-average values \bar{p} . Thus, we will formulate numerical schemes to determine these unknown cell-averages as the numerical approximations to the solutions of the Liouville equations and its adjoints. Without loss of generality, we denote the cell-averages without the bars.

For the control function u, we use a piecewise constant approximation, where we denote with $u^{k+1/2}$ the value of the control in the time interval $[t^k, t^{k+1})$. We then project the continuous u to the corresponding numerical grid by setting $u^{k+1/2} = u(t^k)$. For a function g defined on $Q_{h,\Delta t}$, we also define the discrete norms $\|\cdot\|_{1,h}$ and $\|\cdot\|_{\infty,h}$ as follows:

$$||g(\cdot,\cdot,t^k)||_{1,h} = h^2 \sum_{i,j}^{N_x} |g_{i,j}^k|, \qquad ||g(\cdot,\cdot,t^k)||_{\infty,h} = \max_{i,j=1,\dots,N_x} |g_{i,j}^k|,$$

where $g_{i,j}^k = g(x^i, q^j, t^k)$, and (x^i, q^j, t^k) denotes a grid point in $\Omega \times [0, T]$.

5.1 A Euler-Kurganov-Tadmor scheme for solving the Liouville equations

In this section, we discuss a numerical scheme for solving the Liouville equations (8) and (11) in $\Omega \times [0, T]$. For the spatial discretization, we consider a finite-volume scheme proposed by Kurganov-Tadmor (KT) in [50], combined with a generalized MUSCL flux. To describe this scheme, the flux in the Liouville equations can be considered as a function of p and is denoted by $\mathcal{H}(p) = bp$. Then the KT scheme for the Liouville equation in semi-discretized form is given as follows

$$\frac{\mathrm{d}}{\mathrm{dt}}p_{i,j}(t) = -\frac{F_{i+1/2,j}^{x}(p^{+}, p^{-}; t) - F_{i-1/2,j}^{x}(p^{+}, p^{-}; t)}{h} - \frac{F_{i,j+1/2}^{q}(p^{+}, p^{-}; t) - F_{i,j-1/2}^{q}(p^{+}, p^{-}; t)}{h}, \qquad i, j = 1, \dots, N_{x} - 1, \tag{17}$$

where the $F_{\cdot,\cdot}^x(p^+,p^-;t)$, $F_{\cdot,\cdot}^q(p^+,p^-;t)$ are the numerical fluxes in the x and q directions, respectively. These numerical fluxes are defined as follows:

$$F_{i+1/2,j}^{x}(p^{+},p^{-};t) := \frac{h^{1}(p_{i+1/2,j}^{+}(t)) + h^{1}(\rho_{i+1/2,j}^{-}(t))}{2} - \frac{\mathcal{V}_{i+1/2,j}^{x}(t)}{2} \left[p_{i+1/2,j}^{+}(t) - p_{i+1/2,j}^{-}(t)\right], \tag{18}$$

$$F_{i,j+1/2}^{q}(p^{+},p^{-};t) := \frac{h^{2}(p_{i,j+1/2}^{+}(t)) + h^{2}(\rho_{i,j+1/2}^{-}(t))}{2} - \frac{\mathcal{V}_{i,j+1/2}^{q}(t)}{2} \Big[p_{i,j+1/2}^{+}(t) - p_{i,j+1/2}^{-}(t) \Big], \tag{19}$$

where $\mathcal{H} = (h^1, h^2) = (b^1 p, b^2 p)$. In the aforementioned formulae, the so-called local speeds $\mathcal{V}^x(t)$, $\mathcal{V}^q(t)$ are given by

$$\mathcal{V}_{i+1/2,j}^{x}(t) = \left| b^{1}(x^{i+1/2}, q^{j}, t; u(t)) \right|, \quad \mathcal{V}_{i,j+1/2}^{q}(t) = \left| b^{2}(x^{i}, q^{j+1/2}, t; u(t)) \right|, \quad (20)$$

since $\mathcal{H}(p) = bp$ is linear in p.

The approximation of p at the cell edges in (19) is given by following intermediate values

$$p_{i+1/2,j}^+(t) := p_{i+1,j}(t) - \frac{h}{2}(p_x)_{i+1,j}(t), \qquad p_{i+1/2,j}^-(t) := p_{i,j}(t) + \frac{h}{2}(p_x)_{i,j}(t). \tag{21}$$

The partial derivatives of p are approximated using the minmod function as follows: In direction x, we have

$$(p_x)_{i,j}(t) = \operatorname{minmod}\left(\frac{p_{i,j}(t) - p_{i-1,j}(t)}{h}, \frac{p_{i+1,j}(t) - p_{i-1,j}(t)}{2h}, \frac{p_{i+1,j}(t) - p_{i,j}(t)}{h}\right). \tag{22}$$

An analogous expression holds in the direction q. Here the multivariable minmod function for vectors $x \in \mathbb{R}^d$ is given by

$$\min \operatorname{minmod}(x_1, x_2, \dots, x_d) := \begin{cases} \min_j \{x_j\} & \text{if } x_j > 0, \ \forall j \in [1, d] \\ \max_j \{x_j\} & \text{if } x_j < 0, \ \forall j \in [1, d] \\ 0 & \text{otherwise.} \end{cases}$$

For the time discretization of the Liouville equations (8) and (11), we use the standard first order Euler finite differencing scheme. Together with the KT flux discretization in the spatial variables, we obtain the fully discrete approximation of the Liouville equations that we call as the Euler-KT (EKT) scheme. This scheme is implemented as follows: Given initial condition $p_{i,j}^k$, in (t^k, t^{k+1}) , we have

$$p_{i,j}^{k+1} = p_{i,j}^k + \Delta t \, G(\rho_{i,j}^k). \tag{23}$$

Here, we use the following definition of the fully discrete fluxes

$$G(p_{i,j}^k) = -\frac{F_{i+1/2,j}^{x,k} - F_{i-1/2,j}^{x,k}}{h} - \frac{F_{i,j+1/2}^{q,k} - F_{i,j-1/2}^{q,k}}{h}.$$
 (24)

where $F_{\cdot,\cdot}^{x,k}$, $F_{\cdot,\cdot}^{q,k}$ denotes $F_{\cdot,\cdot}^{x}$, $F_{\cdot,\cdot}^{q}$, as given in (19), corresponding to the time step t^{k} .

We now analyze some properties of the EKT scheme, given in (23). We begin with a strong stability property of the EKT scheme that can be proved using arguments given in [51, Lemma 2.1]

Proposition 5. The EKT scheme has the following strong stability property

$$||p^{k+1}||_{\infty,h} \le ||p^k||_{\infty,h}, \qquad k = 0, \dots, N_t - 1.$$

We next show the conservativeness property of the EKT scheme.

Lemma 5.1 (Conservativeness). The EKT scheme is conservative, in the sense that

$$\sum_{i,j=1}^{N_x} p_{i,j}^k = \sum_{i,j=1}^{N_x} p_{i,j}^0, \qquad k = 1, \dots, N_t.$$

Proof. For a fixed $k \in \{0, ..., N_t\}$, summing up both the sides in (23) over all indices $i, j \in \{1, ..., N_x\}$ and using the fact that the solution has zero flux on the boundary, due to the fact that it has compact support in Ω , we obtain

$$\sum_{i,j=1}^{N_x} p_{i,j}^{k+1} = \sum_{i,j=1}^{N_x} p_{i,j}^k.$$

Iterating over k, we have

$$\sum_{i,j=1}^{N_x} p_{i,j}^k = \sum_{i,j=1}^{N_x} p_{i,j}^0, \qquad k = 1, \dots, N_t$$

which gives us the desired result.

We next show that, under some restriction on Δt , the EKT scheme is positive, i.e., starting with $p_0 \geq 0$, we obtain $p^k \geq 0$ for all k. For this purpose, we define the CFL-number as

$$\lambda := \frac{\Delta t}{h}.\tag{25}$$

We then impose that the function b satisfies the following conditions

$$\lambda \left\| b^1 \right\|_{L^{\infty}(0,T;L^{\infty}(\Omega))} \le \frac{1}{4}, \qquad \lambda \left\| b^2 \right\|_{L^{\infty}(0,T;L^{\infty}(\Omega))} \le \frac{1}{4}. \tag{26}$$

Under the CFL condition (26), we can prove the following lemma on the positivity of the EKT scheme.

Lemma 5.2 (Positivity). Under the CFL-condition (26), the numerical solutions to the Liouville equations (8) and (11), computed with the EKT scheme, given in (23) is non-negative, that is,

$$p_{i,j}^0 \ge 0 \implies p_{i,j}^k \ge 0, \qquad i, j = 1, \dots, N_x, \qquad k = 1, \dots, N_t.$$
 (27)

Proof. Let $p_{i,j}^k \ge 0$ for fixed $0 \le k < N_t$. We will show that $p_{i,j}^{k+1} \ge 0$ for all $i, j = 1, \dots, N_x$. For this purpose, we note that the EKT scheme can be written alternatively in the following form

$$p_{i,j}^{k+1} = \frac{\lambda}{2} (|b_{i+1/2,j}^{1}| - b_{i+1/2,j}^{1}) p_{i+1/2,j}^{+} + \frac{\lambda}{2} (|b_{i-1/2,j}^{1}| + b_{i-1/2,j}^{1}) p_{i-1/2,j}^{-} + \frac{\lambda}{2} (|b_{i,j+1/2}^{2}| - b_{i,j+1/2}^{2}) p_{i,j+1/2}^{+} + \frac{\lambda}{2} (|b_{i,j-1/2}^{2}| + b_{i,j-1/2}^{2}) p_{i,j-1/2}^{-} + \left[\frac{1}{4} - \frac{\lambda}{2} (|b_{i+1/2,j}^{1}| + b_{i+1/2,j}^{1}) \right] p_{i+1/2,j}^{-} + \left[\frac{1}{4} - \frac{\lambda}{2} (|b_{i-1/2,j}^{1}| - b_{i-1/2,j}^{1}) \right] p_{i-1/2,j}^{+} + \left[\frac{1}{4} - \frac{\lambda}{2} (|b_{i,j+1/2}^{2}| + b_{i,j+1/2}^{2}) \right] p_{i,j+1/2}^{-} + \left[\frac{1}{4} - \frac{\lambda}{2} (|b_{i,j-1/2}^{2}| - b_{i,j-1/2}^{2}) \right] p_{i,j-1/2}^{+}$$

$$(28)$$

where all discrete quantities on the right are considered at the timestep t^k . We note that if $\rho_{i\pm 1/2,j}^{\pm}$, $\rho_{i,j\pm 1/2}^{\pm} \geq 0$, then the first four terms on the right hand side in (28) are always non-negative. The other terms are non-negative under the CFL-condition (26). Thus, we only need to show that $p_{i+1/2,j}^{\pm}$, $p_{i,j+1/2}^{\pm} \geq 0$ for all $i, j = 1, \ldots, N_x$, where $p_{i,j}^{\pm}$ is given as in (21).

For this purpose, we will consider each expression of $(p_x)_{i,j}^k$, given in (22)(a similar analysis also holds for $(p_q)_{i,j}^k$). For the first case, we assume $(p_x)_{i,j}^k = \frac{p_{i,j}^k - p_{i-1,j}^k}{h}$. We then have

$$p_{i+1/2,j}^+ = \frac{1}{2}p_{i+1,j}^k + \frac{1}{2}p_{i,j}^k,$$

which is non-negative, since $p_{i,j}^k \geq 0$ for all $i,j=1,\ldots,N_x$. We also have, $p_{i+1/2,j}^- = p_{i,j}^k + \frac{h}{2} \left[\frac{p_{i,j}^k - p_{i-1,j}^k}{h} \right]$. If $\frac{p_{i,j}^k - p_{i-1,j}^k}{h} > 0$, we then have $p_{i+1/2,j}^- > 0$. On the other hand, if $\frac{p_{i,j}^k - p_{i-1,j}^k}{h} < 0$, then by the definition of the minmod limiter, we have $\frac{p_{i,j}^k - p_{i-1,j}^k}{h} \geq \frac{p_{i+1,j}^k - p_{i,j}^k}{h}$. This implies

$$p_{i+1/2,j}^- \ge p_{i,j}^k + \frac{h}{2} \left\lceil \frac{p_{i+1,j}^k - p_{i,j}^k}{h} \right\rceil = \frac{p_{i+1,j}^k + p_{i,j}^k}{2} \ge 0.$$

The other cases for the value of $(p_x)_{i,j}^k \neq 0$ follow analogously. If $(p_x)_{i,j}^k = 0$, then $p_{i+1/2,j}^{\pm} = p_{i+1,j} \geq 0$ and $p_{i,j+1/2}^{\pm} = p_{i,j+1} \geq 0$. This completes the proof.

We next prove the discrete L^1 stability of the EKT scheme.

Lemma 5.3 (Stability). The solution $p_{i,j}^k$ obtained with the EKT-scheme in (23) is discrete L^1 stable in the sense that

$$\|p_{\cdot,\cdot}^k\|_{1,h} = \|p_{\cdot,\cdot}^0\|_{1,h}, \qquad k = 1,\dots, N_t,$$

under the CFL condition (26).

Proof. The conservativeness property in Lemma 5.1 implies

$$\sum_{i,j=0}^{N_x} p_{i,j}^k = \sum_{i,j=0}^{N_x} p_{i,j}^0, \qquad k = 1, \dots, N_t.$$

The positivity property from Lemma 5.2 implies

$$\sum_{i,j=0}^{N_x} |p_{i,j}^k| = \sum_{i,j=0}^{N_x} |p_{i,j}^0|, \qquad k = 1, \dots, N_t,$$

which proves the desired result.

We next aim at proving the L^1 convergence of the EKT scheme. For this purpose, we state the following stability result, whose proof can be found in [49].

Lemma 5.4. Let $p_{i,j}^k$ be the numerical solution to the Liouville equations (8) and (11), with a Lipschitz continuous right-hand side g(x,q,t), obtained with the EKT scheme. Then under the CFL condition (26), this solution satisfies the following stability estimate

$$\|p_{\cdot,\cdot}^{k+1}\|_{1,h} \le \|p_{\cdot,\cdot}^0\|_{1,h} + \Delta t \sum_{m=0}^k \|g_{\cdot,\cdot}^m\|_{1,h},$$

where $g_{i,j}^m = g(x^i, q^j, t^m)$.

We now consider the local consistency error of our EKT at the point (x^i, q^j, t^k) defined as

$$T_{i,j}^k = \frac{p(x^i, q^j, t^{k+1}) - p(x^i, q^j, t^k)}{\Delta t} + \frac{1}{2h} (L_i^k + L_j^k) (p(x^i, q^j, t^k)) - g_{i,j}^k,$$

where

$$\begin{split} L_i^k(p) = & \left(|b_{i+1/2,j}^1| - b_{i+1/2,j}^1 \right) p_{i+1/2,j}^{k+} - \left(|b_{i+1/2,j}^1| + b_{i+1/2,j}^1 \right) p_{i+1/2,j}^{k-} \\ & + \left(|b_{i-1/2,j}^1| + b_{i-1/2,j}^1 \right) p_{i-1/2,j}^{k-} - \left(|b_{i-1/2,j}^1| - b_{i-1/2,j}^1 \right) p_{i-1/2,j}^{k+}, \\ L_j^k(p) = & \left(|b_{i,j+1/2}^2| - b_{i,j+1/2}^2 \right) p_{i,j+1/2}^{k+} - \left(|b_{i,j+1/2}^2| + b_{i,j+1/2}^2 \right) p_{i,j+1/2}^{k-} \\ & + \left(|b_{i,j-1/2}^2| + b_{i,j-1/2}^2 \right) p_{i,j-1/2}^{k-} - \left(|b_{i,j-1/2}^2| - b_{i,j-1/2}^2 \right) p_{i,j-1/2}^{k+} \end{split}$$

The accuracy result for the KT scheme, given in [49], the MUSCL reconstruction error given in Equation (60) in [52, Section 4.4] for the case when $\kappa = 0$, give us the following result

Lemma 5.5. Let $p \in C^3$ be the exact solution of the Liouville equations (8) and (11) Under the CFL condition (26), the consistency error $T_{i,j}^k$ satisfies the following error estimate

$$|T_{i,j}^k| = \mathcal{O}(h^2) + \mathcal{O}(\Delta t)$$

except possibly at the points of extrema of p where the consistency error can be first-order in h.

We now define the error at the point (x^i, q^j, t^k) as

$$e_{i,j}^k = p_{i,j}^k - p(x^i, q^j, t^k).$$

We then note that e satisfies (23) with the source term given by $-T_{i,j}^k$. Lemma 5.4 gives us

$$\|e_{\cdot,\cdot}^{k+1}\|_{1,h} \le \|e_{\cdot,\cdot}^0\|_{1,h} + \Delta t \sum_{m=0}^k \|T_{\cdot,\cdot}^m\|_{1,h}.$$

With the aforementioned preparation, we now have the following result on the L^1 convergence of the solution obtained using the EKT scheme.

Theorem 5.1. Let $p \in C^3$ be the exact solution of the Liouville equations (8) and (11), with finite many extrema, and let $\|p_{\cdot,\cdot}^0 - p_0(\cdot,\cdot)\|_{1,h} = \mathcal{O}(h)$. Under the CFL condition (26), the solution $p_{i,j}^k$ obtained with the EKT scheme, given by (23), is first-order accurate in the discrete L^1 -norm as follows

$$\|p_{\cdot,\cdot}^k - \rho(\cdot,\cdot,t^k)\|_{1,h} \le D(T,\Omega,\lambda) h.$$

For the adjoint equations (ADJ:LIOUV) and (ADJU:LIOUV), we first convert the equations into a divergence form, which results in additional zeroth order terms in w. We then use the Euler time discretization and the KT spatial derivative discretization to solve the adjoint equations numerically. For the optimization problems, we use a well-known gradient-based algorithm called the nonlinear conjugate gradient (NCG) algorithm. The NCG algorithm can be used to solve both the parameter estimation (finite-dimensional) and optimal treatment (infinite dimensional) optimization problems using a modified gradient update step,

where the descent directions are modified from the negative gradient directions, leading to faster and accurate solutions of the optimality system compared to the traditional gradient descent method. Such a method has been used in past in context of solving parameter estimation and optimal treatment problems in colon and esophageal cancer cancer [28, 53, 29], crowd-motion control problems [54, 42, 55, 56], and parameter estimation problems related to statistical cure rate models [57, 58, 59]. We also remark that besides the NCG and the associated class of gradient based methods for solving optimal control problems, there are other classes of optimal control algorithms that are based on approximations of the optimality system using basis functions, e.g., pseudospectral methods [60, 61] and the control parameterization methods [62, 63], which also might be used as an alternate solution method for the proposed optimal treatment problem.

6 Numerical results

In this section, we present the results of numerical simulations with the Liouville parameter estimation and optimal control frameworks. For the parameter estimation problem, given in (10), we choose our domain $\Omega = (0,6)^2$ and discretize it using $N_x = 51$ points. The final time t is chosen to be 1.0 and the maximum number of time steps N_t is chosen to be 1000. We generate the patient data, using different true parameter values of θ , by first considering target PDFs $p_i^d(x)$, $i = 1, \dots, N$ with N = 100, where p_i^d are described by a normal distribution about the measured mean value $\mathbb{E}[p_i^d]$ and variance 0.05. We then use a 3D interpolation to obtain the data function $p^d(x, q, t)$ at all discrete times t_k , $k = 1, \dots, N_t$. The regularization parameters are chosen to be $\alpha = 1$, $\beta = 0.1$.

6.1 Parameter estimation results

Test Case 1: In the first test case, the true parameters and the initial guess for the NCG algorithm are given in Table 2. We then solve the Liouville parameter estimation problem, given in (10). For comparison purposes, we use the reduced ODE system (7) and use the parameter estimation framework similar to as presented in Section 3.1 by solving the following constrained optimization problem

$$\min_{\theta \in T_{ad}} J(X, Q, \theta) = \frac{\alpha}{2} \int_0^T \left[(X(t) - X^d(t))^2 + (Q(t) - Q^d(t))^2 \right] dt + \frac{\beta}{2} \|\theta\|^2, \tag{29}$$

subject to the ODE system (7). The results of this comparison are shown in Figure 2.

Parameters	μ_m	d	s	A
True	3.3	1.7	0.9	3.9
Guess	2.5	0.5	0.1	3

Table 2: Test case 1: Patient-specific parameter values

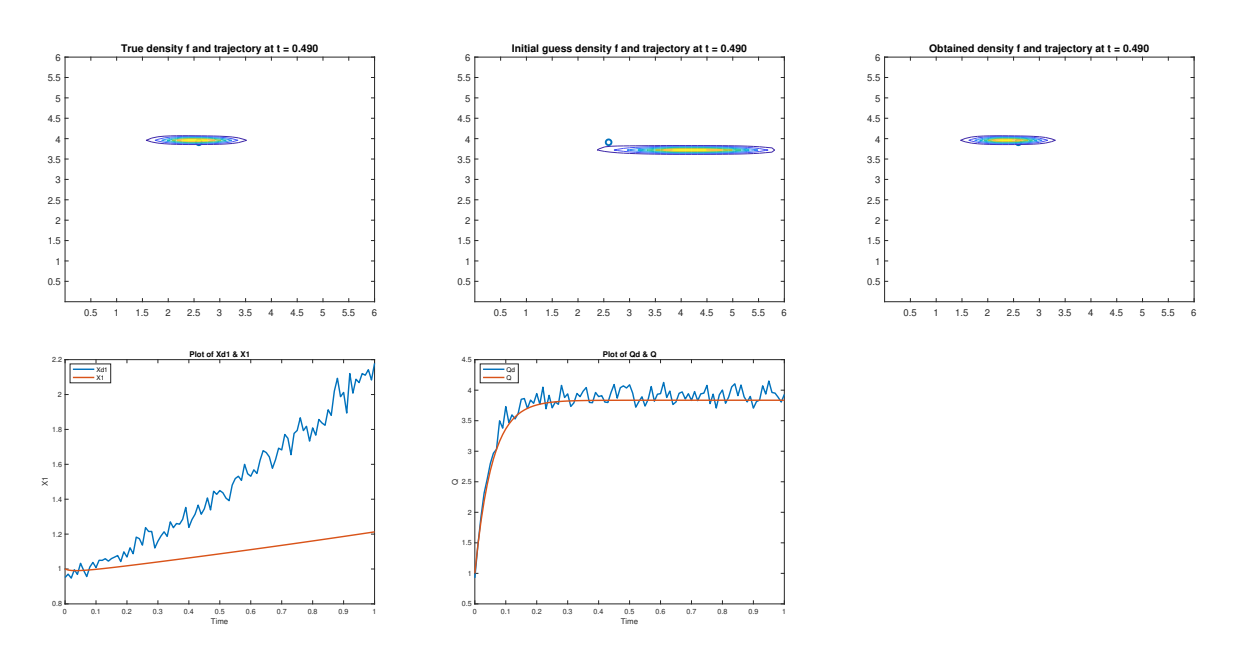


Figure 2: Test Case 1: Comparison between the ODE and Liouville parameter estimation case

In the first row of Figure 2, the first figure represents the PDF obtained by solving the Liouville equation (8) with the true parameters at t=0.49. The small dot represents the corresponding trajectory point of the ODE (7) and is at the same location across all the figures in the first row. We note that the center of the PDF approximately matches the trajectory point, which is because the expected value of the Liouville PDF should give the solution of the ODE (7). The second figure in the first row represents the PDF obtained by using the initial guess for the parameters. We note that the center of this PDF does not match the trajectory point, which means we are not close to the true parameters. By solving the parameter estimation problem, we obtain the PDF in the third figure of the first row whose center now is very close to the trajectory point. On the other hand, the ODE parameter estimation framework results are shown in the second row and we clearly see that the trajectory for the X variable does not resemble the true trajectory. This implies the accuracy of our Liouville parameter estimation framework over the ODE parameter estimation framework.

Test Case 2: In our second test case, we now have a set of different true parameters and, correspondingly, different initial guesses, given in Table 3.

Parameters	μ_m	d	s	A
True	3.5	1.9	1.1	3.9
Initial guess	4	1.0	0.5	3.0

Table 3: Test case 2: Patient-specific parameter values

We again perform a comparison between the Liouville parameter estimation framework

and the ODE parameter estimation framework. The results are shown in Figure 3.

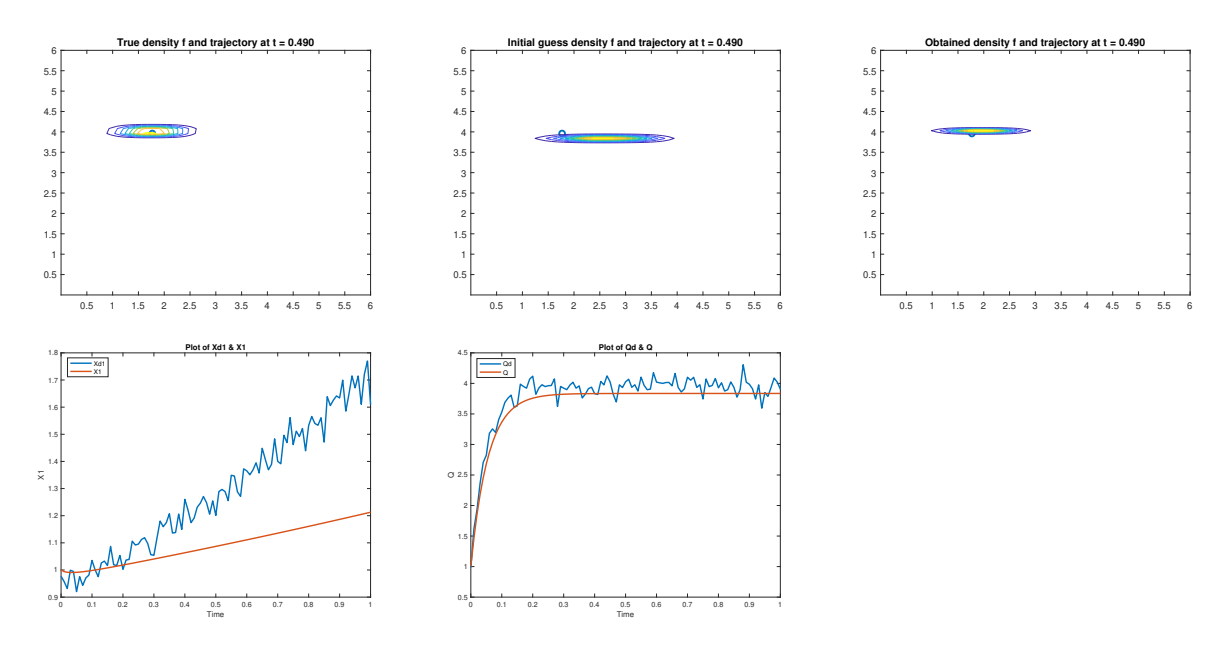


Figure 3: Test Case 2: Comparison between the ODE and Liouville parameter estimation case.

Using a similar analysis as in Test Case 1, we again note that the Liouville parameter estimation framework provides more accurate results as compared to the ODE parameter estimation framework. We also compute the respective relative L^2 errors for the 2 test cases. The relative L^2 error between 2 functions X(t) and $X^d(t)$ is defined as

$$Err(X, X^d) = \frac{\|X - X^d\|_{L_2([0,T])}}{\|X^d\|_{L_2([0,T])}},$$

whereas the relative L^2error between 2 functions p(x,q,t) and $p^d(x,q,t)$ is defined as

$$Err_p(p, p^d) = \frac{\|p - p^d\|_{L_2(\Omega \times [0, T])}}{\|p^d\|_{L_2(\Omega \times [0, T])}}$$

 Test Case
 $Err(X^1, X_1^d)$ $Err(Q, Q^d)$ $Err_p(p, p^d)$

 1
 0.4761
 0.0803
 0.1314

 2
 0.3312
 0.0347
 0.1219

Table 4: L^2 error table

From Table 4, we observe that the error between the ODE solution (X^1, Q^1) and the data is far more higher than the corresponding difference between the Liouville PDF p and the data function p^d . This further shows that the Liouville modeling and parameter estimation framework is more accurate than the ODE framework.

6.2 Optimal control results

We now present the results of our optimal control framework. For this purpose, we consider the patient-specific parameters obtained from Test Case 1 in Section 6.1. We then considered a PDF along a desired trajectory and the goal of the optimal control problem is to drive the uncontrolled PDF to the desired PDF. We consider two such cases whose plots are shown in Figures 4 and 5.

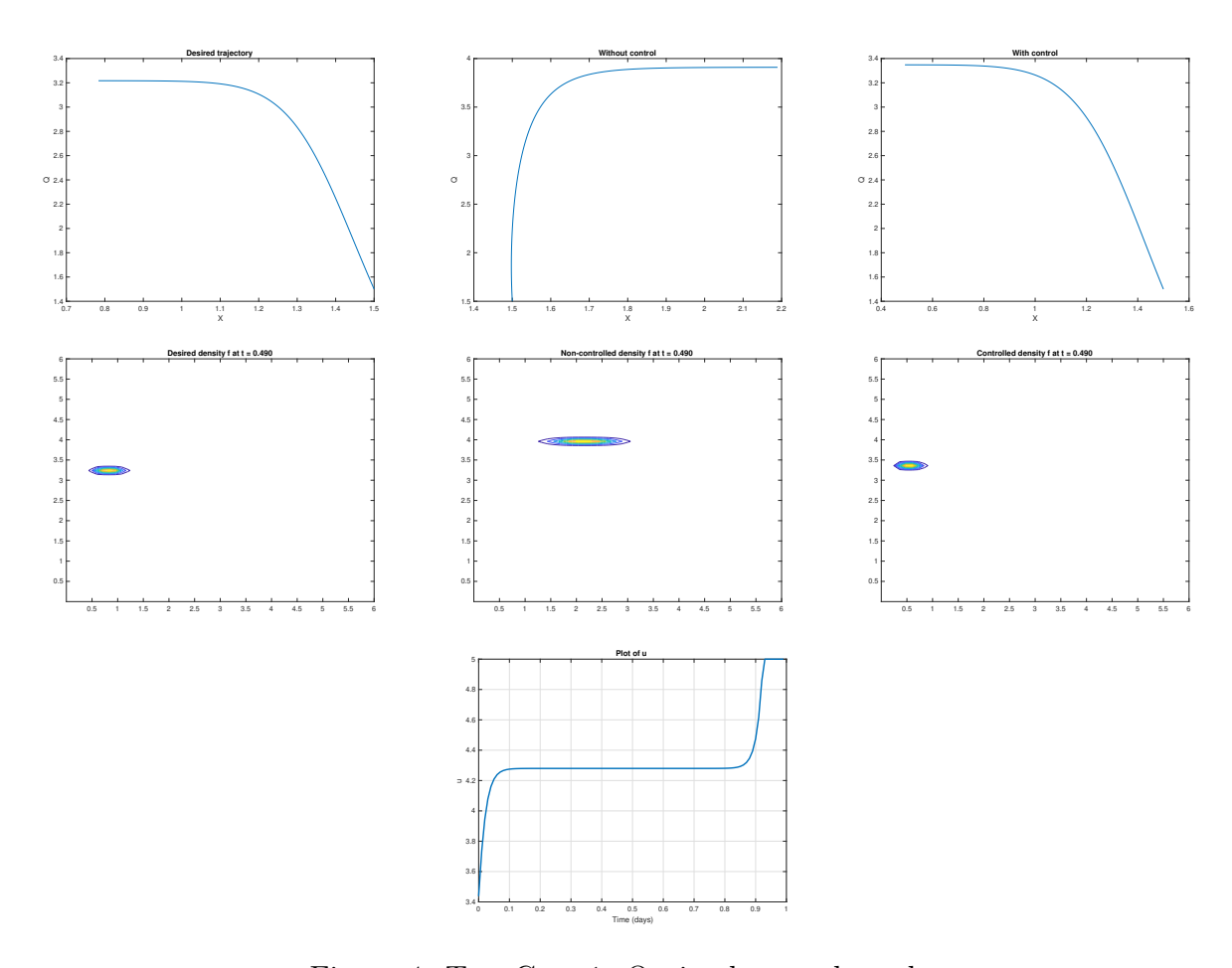


Figure 4: Test Case 1: Optimal control results

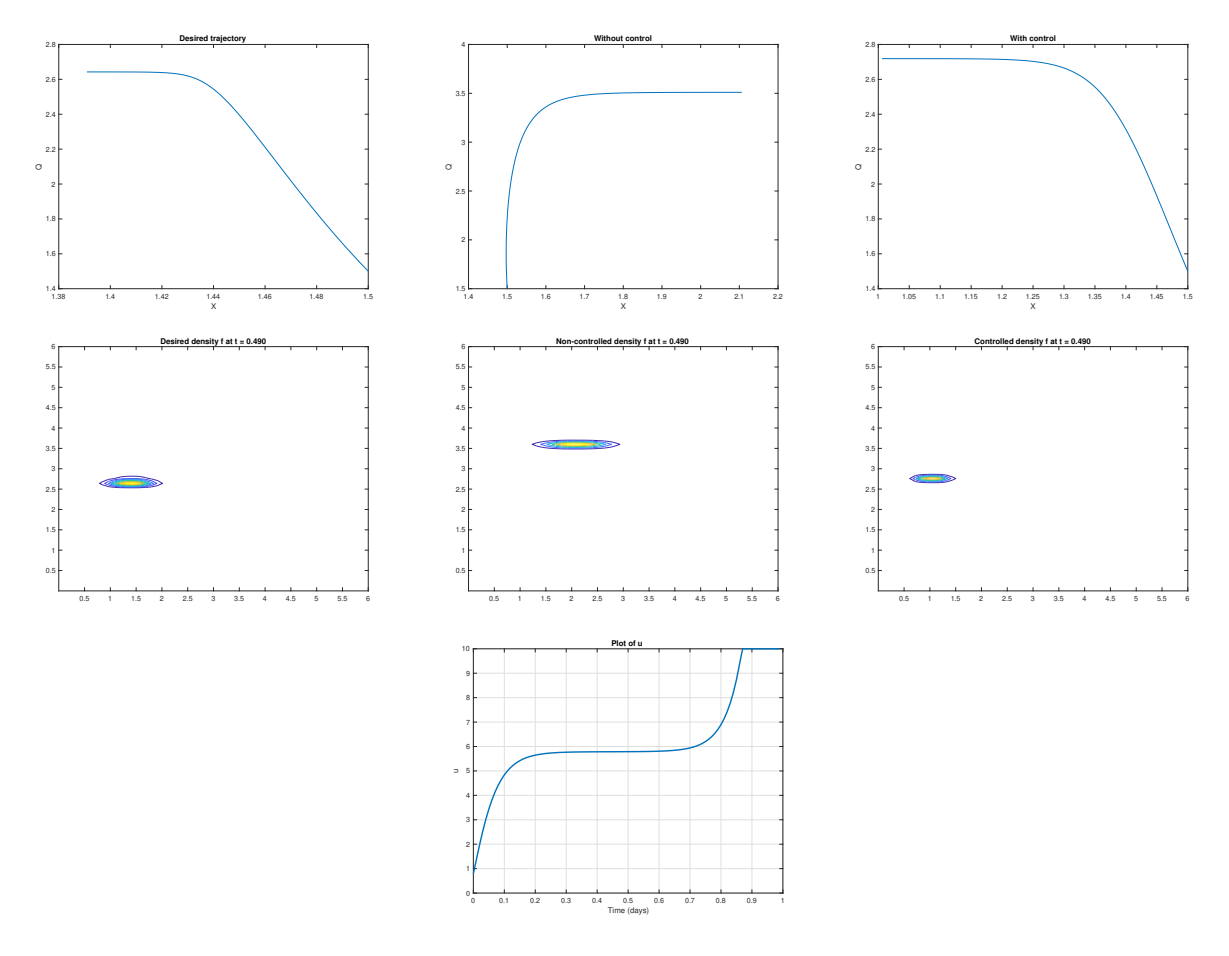


Figure 5: Test Case 2: Optimal control results

In each set of plots, the first row is composed of three figures. The first figure represents the desired trajectory, the second figure represents the trajectory without control, and the third figure represents the trajectory with control strategies. Progressing to the following row, again composed of three figures, the first figure represents the desired Probability Density Function (PDF) at the specific time point of t = 0.49. The second figure in this row represents the PDF without control, and the last figure represents the controlled PDF. Concluding the sequence, the last row contains the plot of the controls.

We observe that in both cases, the control drives the PDF to the desired state in an accurate way. The major difference between the two test cases is the asymptotic level of the desired value of Q, which is lower in the second case. For this reason, we also observe that the control value is higher in the second case compared to the first case.

7 Conclusions

In this chapter, we have presented a Liouville framework for parameter estimation and optimal control in prostate cancer. The main rationale behind this framework is the uncertainty in carrying out similar trials in a given environment, which leads to random evolution mechanisms. We presented a comparison of the Liouville parameter estimation framework and the ODE parameter estimation framework, and demonstrated that the Liouville parameter

rameter estimation framework provides a more accurate and robust parameter estimation technique. Finally, we also implemented the Liouville optimal control framework and the results validated the robustness and accuracy of our proposed methods.

8 Acknowledgements

S. Roy was partly funded by the US National Science Foundation grant numbers 2212938 and 2230790.

References

- [1] Ahmedin Jemal, Rebecca Siegel, Elizabeth Ward, Yongping Hao, Jiaquan Xu, and Michael J Thun. Cancer statistics, 2009. *CA: a cancer journal for clinicians*, 59(4):225–249, 2009.
- [2] Ahmedin Jemal, Rebecca Siegel, Elizabeth Ward, Yongping Hao, Jiaquan Xu, Taylor Murray, and Michael J Thun. Cancer statistics, 2008. *CA: a cancer journal for clinicians*, 58(2):71–96, 2008.
- [3] Cyrus Washington, Daniel A Goldstein, Assaf Moore, Ulysses Gardner Jr, and Curtiland Deville Jr. Health disparities in prostate cancer and approaches to advance equitable care. American Society of Clinical Oncology Educational Book, 42:360–365, 2022.
- [4] Harold Evelyn Taitt. Global trends and prostate cancer: a review of incidence, detection, and mortality as influenced by race, ethnicity, and geographic location. *American journal of men's health*, 12(6):1807–1823, 2018.
- [5] Mohammad Norouzi, Mehrnaz Amerian, Mahshid Amerian, and Fatemeh Atyabi. Clinical applications of nanomedicine in cancer therapy. *Drug discovery today*, 25(1):107–125, 2020.
- [6] Wu Zhou, Yan Jiang, LL Ji, Lianlian Zhou, Meijuan Zhang, Mo Shen, Jia Zhao, Hongxiang Tu, Zhongyong Wang, Ruihao Wu, et al. Expression profiling of genes in androgen metabolism in androgen-independent prostate cancer cells under an androgen-deprived environment: mechanisms of castration resistance. *International Journal Of Clinical And Experimental Pathology*, 9:8424–31, 2016.
- [7] Carmen Bax, Gianluigi Taverna, Lidia Eusebio, Selena Sironi, Fabio Grizzi, Giorgio Guazzoni, and Laura Capelli. Innovative diagnostic methods for early prostate cancer detection through urine analysis: A review. *Cancers*, 10(4):123, 2018.
- [8] Leonid Hanin and Marco Zaider. Effects of surgery and chemotherapy on metastatic progression of prostate cancer: evidence from the natural history of the disease reconstructed through mathematical modeling. *Cancers*, 3(3):3632–3660, 2011.
- [9] Michael F Leitzmann and Sabine Rohrmann. Risk factors for the onset of prostatic cancer: age, location, and behavioral correlates. *Clinical epidemiology*, pages 1–11, 2012.

- [10] Yang Kuang, John D Nagy, and Steffen E Eikenberry. *Introduction to mathematical oncology*. CRC Press, 2018.
- [11] Tin Phan, Sharon M Crook, Alan H Bryce, Carlo C Maley, Eric J Kostelich, and Yang Kuang. Mathematical modeling of prostate cancer and clinical application. *Applied Sciences*, 10(8):2721, 2020.
- [12] Aiko Miyamura Ideta, Gouhei Tanaka, Takumi Takeuchi, and Kazuyuki Aihara. A mathematical model of intermittent androgen suppression for prostate cancer. *Journal of nonlinear science*, 18:593–614, 2008.
- [13] Travis Portz, Yang Kuang, and John D Nagy. A clinical data validated mathematical model of prostate cancer growth under intermittent androgen suppression therapy. *Aip Advances*, 2(1):011002, 2012.
- [14] Erica M Rutter and Yang Kuang. Global dynamics of a model of joint hormone treatment with dendritic cell vaccine for prostate cancer. *DCDS-B*, 22(3):1001–1021, 2017.
- [15] Javier Baez and Yang Kuang. Mathematical models of androgen resistance in prostate cancer patients under intermittent androgen suppression therapy. *Applied Sciences*, 6(11):352, 2016.
- [16] Jinqiao Duan. An introduction to stochastic dynamics, volume 51. Cambridge University Press, 2015.
- [17] Harsh Vardhan Jain, Steven K Clinton, Arvinder Bhinder, and Avner Friedman. Mathematical modeling of prostate cancer progression in response to androgen ablation therapy. *Proceedings of the National Academy of Sciences*, 108(49):19701–19706, 2011.
- [18] Assia Zazoua and Wendi Wang. Analysis of mathematical model of prostate cancer with androgen deprivation therapy. Communications in Nonlinear Science and Numerical Simulation, 66:41–60, 2019.
- [19] Charles Huggins and Clarence V Hodges. Studies on prostatic cancer: I. the effect of castration, of estrogen and of androgen injection on serum phosphatases in metastatic carcinoma of the prostate. *The Journal of urology*, 168(1):9–12, 2002.
- [20] Satish Kumar, Mike Shelley, Craig Harrison, Bernadette Coles, Timothy J Wilt, and Malcolm Mason. Neo-adjuvant and adjuvant hormone therapy for localised and locally advanced prostate cancer. *Cochrane Database of Systematic Reviews*, (4), 2006.
- [21] Dominick GA Burton, Maria G Giribaldi, Anisleidys Munoz, Katherine Halvorsen, Asmita Patel, Merce Jorda, Carlos Perez-Stable, and Priyamvada Rai. Androgen deprivation-induced senescence promotes outgrowth of androgen-refractory prostate cancer cells. *PloS one*, 8(6):e68003, 2013.
- [22] L Klotz and P Toren. Androgen deprivation therapy in advanced prostate cancer: is intermittent therapy the new standard of care? Current oncology, 19(s1):13–21, 2012.

- [23] Johannes M Wolff, Per-Anders Abrahamsson, Jacques Irani, and Fernando Calais da Silva. Is intermittent androgen-deprivation therapy beneficial for patients with advanced prostate cancer? *BJU international*, 114(4):476–483, 2014.
- [24] Tobias Engel Ayer Botrel, Otávio Clark, Rodolfo Borges Dos Reis, Antônio Carlos Lima Pompeo, Ubirajara Ferreira, Marcus Vinicius Sadi, and Francisco Flávio Horta Bretas. Intermittent versus continuous androgen deprivation for locally advanced, recurrent or metastatic prostate cancer: a systematic review and meta-analysis. BMC urology, 14:1– 14, 2014.
- [25] Martin Gleave, Laurence Klotz, and Samir S Taneja. The continued debate: intermittent vs. continuous hormonal ablation for metastatic prostate cancer. In *Urologic Oncology: Seminars and Original Investigations*, volume 27, pages 81–86. Elsevier, 2009.
- [26] George W Swan and Thomas L Vincent. Optimal control analysis in the chemotherapy of igg multiple myeloma. *Bulletin of mathematical biology*, 39:317–337, 1977.
- [27] Urszula Ledzewicz and Heinz Schaettler. Optimizing chemotherapeutic anti-cancer treatment and the tumor microenvironment: an analysis of mathematical models. Systems Biology of Tumor Microenvironment: Quantitative Modeling and Simulations, pages 209–223, 2016.
- [28] Souvik Roy and Suvra Pal. Optimal personalized therapies in colon cancer induced immune response using a fokker-planck framework. *Mathematics and Computer Science Volume 2*, pages 33–47, 2023.
- [29] Souvik Roy, Zui Pan, and Suvra Pal. A fokker–planck feedback control framework for optimal personalized therapies in colon cancer-induced angiogenesis. *Journal of Mathematical Biology*, 84(4):23, 2022.
- [30] Yoshito Hirata and Kazuyuki Aihara. Ability of intermittent androgen suppression to selectively create a non-trivial periodic orbit for a type of prostate cancer patients. *Journal of theoretical biology*, 384:147–152, 2015.
- [31] Yoshito Hirata, Kai Morino, Koichiro Akakura, Celestia S Higano, and Kazuyuki Aihara. Personalizing androgen suppression for prostate cancer using mathematical modeling. *Scientific reports*, 8(1):2673, 2018.
- [32] Jessica J Cunningham, Joel S Brown, Robert A Gatenby, and Kateřina Staňková. Optimal control to develop therapeutic strategies for metastatic castrate resistant prostate cancer. *Journal of theoretical biology*, 459:67–78, 2018.
- [33] Frederico Leal, Maximiliano Augusto Novis de Figueiredo, and Andre Deeke Sasse. Optimal duration of androgen deprivation therapy following radiation therapy in intermediate-or high-risk non-metastatic prostate cancer: A systematic review and meta-analysis. *International braz j urol*, 41:425–434, 2015.

- [34] Motohiro Murakami, Hitoshi Ishikawa, Shosei Shimizu, Hiromitsu Iwata, Tomoaki Okimoto, Masaru Takagi, Shigeyuki Murayama, Tetsuo Akimoto, Hitoshi Wada, Takeshi Arimura, et al. Optimal androgen deprivation therapy combined with proton beam therapy for prostate cancer: results from a multi-institutional study of the japanese radiation oncology study group. *Cancers*, 12(6):1690, 2020.
- [35] Shabbir MH Alibhai, Efthymios Papadopoulos, Sara Durbano, George Tomlinson, Daniel Santa Mina, Paul Ritvo, Catherine M Sabiston, Andrew G Matthew, James Chiarotto, Souraya Sidani, et al. Preference-based versus randomized controlled trial in prostate cancer survivors: Comparison of recruitment, adherence, attrition, and clinical outcomes. Frontiers in Oncology, 12:1033229, 2022.
- [36] Michael J Grayling, Munyaradzi Dimairo, Adrian P Mander, and Thomas F Jaki. A review of perspectives on the use of randomization in phase ii oncology trials. *JNCI: Journal of the National Cancer Institute*, 111(12):1255–1262, 2019.
- [37] Nicola Mills, Jenny L Donovan, Monica Smith, Ann Jacoby, David E Neal, and Freddie C Hamdy. Perceptions of equipoise are crucial to trial participation: a qualitative study of men in the protect study. *Controlled clinical trials*, 24(3):272–282, 2003.
- [38] Rongbin Ge, Zongwei Wang, and Liang Cheng. Tumor microenvironment heterogeneity an important mediator of prostate cancer progression and therapeutic resistance. NPJ precision oncology, 6(1):31, 2022.
- [39] Souvik Roy and Alfio Borzì. Numerical investigation of a class of liouville control problems. *Journal of Scientific Computing*, 73:178–202, 2017.
- [40] Fatiha Alabau-Boussouira, Roger Brockett, Olivier Glass, Jérôme Le Rousseau, Enrique Zuazua, and Roger Brockett. Notes on the control of the liouville equation. Control of Partial Differential Equations: Cetraro, Italy 2010, Editors: Piermarco Cannarsa, Jean-Michel Coron, pages 101–129, 2012.
- [41] Roger W Brockett. Optimal control of the liouville equation. AMS IP Studies in Advanced Mathematics, 39:23, 2007.
- [42] Souvik Roy, Mario Annunziato, and Alfio Borzì. A fokker–planck feedback control-constrained approach for modelling crowd motion. *Journal of Computational and Theoretical Transport*, 45(6):442–458, 2016.
- [43] RA Everett, AM Packer, and Yang Kuang. Can mathematical models predict the outcomes of prostate cancer patients undergoing intermittent androgen deprivation therapy? *Biophysical Reviews and Letters*, 9(02):173–191, 2014.
- [44] Richard R Berges, Jasminka Vukanovic, Jonathan I Epstein, Marne CarMichel, Lars Cisek, Douglas E Johnson, Robert W Veltri, Patrick C Walsh, and John T Isaacs. Implication of cell kinetic changes during the progression of human prostatic cancer. Clinical cancer research: an official journal of the American Association for Cancer Research, 1(5):473–480, 1995.

- [45] Nicholas Bruchovsky, Laurence Klotz, Juanita Crook, and S Larry Goldenberg. Locally advanced prostate cancer—biochemical results from a prospective phase ii study of intermittent androgen suppression for men with evidence of prostate-specific antigen recurrence after radiotherapy. Cancer: Interdisciplinary International Journal of the American Cancer Society, 109(5):858–867, 2007.
- [46] Tin Phan, Kyle Nguyen, Preeti Sharma, and Yang Kuang. The impact of intermittent androgen suppression therapy in prostate cancer modeling. *Applied Sciences*, 9(1):36, 2018.
- [47] Jan Bartsch, Alfio Borzì, Francesco Fanelli, and Souvik Roy. A theoretical investigation of Brockett's ensemble optimal control problems. *Calc. Var. Partial Differential Equations*, 58(5):34, 2019.
- [48] Jacques-Louis Lions. Quelques méthodes de résolution de problemes aux limites non linéaires. 1969.
- [49] Jan Bartsch, Alfio Borzì, Francesco Fanelli, and Souvik Roy. A numerical investigation of brockett's ensemble optimal control problems. *Numerische Mathematik*, 149(1):1–42, 2021.
- [50] Alexander Kurganov and Eitan Tadmor. New high-resolution central schemes for nonlinear conservation laws and convection-diffusion equations. *J. Comput. Phys.*, 160(1):241–282, 2000.
- [51] Sigal Gottlieb and Chi-Wang Shu. Total variation diminishing Runge-Kutta schemes. *Mathematics of computation*, 67(221):73–85, 1998.
- [52] Hiroaki Nishikawa. A truncation error analysis of third-order muscl scheme for nonlinear conservation laws. *International Journal for Numerical Methods in Fluids*, 2020.
- [53] Souvik Roy, Zui Pan, Naif Abu Qarnayn, Mesfer Alajmi, Ali Alatawi, Asma Alghamdi, Ibrahem Alshaoosh, Zahra Asiri, Berlinda Batista, Shreshtha Chaturvedi, et al. A robust optimal control framework for controlling aberrant rtk signaling pathways in esophageal cancer. *Journal of Mathematical Biology*, 88(2):14, 2024.
- [54] Muhammad Munir Butt and Souvik Roy. A numerical scheme to solve fokker–planck control collective-motion problem. *Mathematics and Computers in Simulation*, 2023.
- [55] Souvik Roy, Mario Annunziato, Alfio Borzì, and Christian Klingenberg. A fokker-planck approach to control collective motion. *Computational Optimization and Applications*, 69:423–459, 2018.
- [56] Souvik Roy, Alfio Borzì, and Abderrahamane Habbal. Pedestrian motion constrained by fp-constrained nash games. Royal Society Open Science, 4(9):170648, 2017.
- [57] Suvra Pal and Souvik Roy. On the estimation of destructive cure rate model: a new study with exponentially weighted poisson competing risks. *Statistica Neerlandica*, 75(3):324–342, 2021.

- [58] Suvra Pal and Souvik Roy. A new non-linear conjugate gradient algorithm for destructive cure rate model and a simulation study: illustration with negative binomial competing risks. Communications in Statistics-Simulation and Computation, 51(11):6866–6880, 2022.
- [59] Suvra Pal and Souvik Roy. On the parameter estimation of box-cox transformation cure model. *Statistics in Medicine*, 42(15):2600–2618, 2023.
- [60] Lorenz T Biegler. An overview of simultaneous strategies for dynamic optimization. Chemical Engineering and Processing: Process Intensification, 46(11):1043–1053, 2007.
- [61] Yan Gao, Zhengyu Wei, Zhijiang Shao, Weifeng Chen, Zhengyu Song, and Lorenz T Biegler. Enhanced moving finite element method based on error geometric estimation for simultaneous trajectory optimization. *Automatica*, 147:110711, 2023.
- [62] Bin Li, Yang Wang, Kai Zhang, and Guang-Ren Duan. Constrained feedback control for spacecraft reorientation with an optimal gain. *IEEE Transactions on Aerospace and Electronic Systems*, 57(6):3916–3926, 2021.
- [63] Bin Li, Tao Guan, Xiaoyi Guan, Kai Zhang, and Ka-Fai Cedric Yiu. Optimal fixed-time sliding mode control for spacecraft constrained reorientation. *IEEE Transactions on Automatic Control*, 69(4):2676–2683, 2024.